




Linear and nonlinear optical properties of CdSe/ZnTe core/shell nanostructures with screened modified Kratzer potential

M. Jaouane^{1,a}, K. El-Bakkari^{1,b}, E. B. Al^{2,c}, A. Sali^{1,d}, F. Ungan^{2,e} 

¹ Laboratory of Solid-State Physics (LPS), Department of Physics, Faculty of Science Dhar El Mahraz, Sidi Mohamed Ben Abdellah University, 1796 Fez, Morocco

² Department of Physics, Faculty of Science, Sivas Cumhuriyet University, 58140 Sivas, Turkey

Received: 29 November 2022 / Accepted: 27 March 2023

© The Author(s), under exclusive licence to Società Italiana di Fisica and Springer-Verlag GmbH Germany, part of Springer Nature 2023

Abstract In this work, we have theoretically examined the linear, nonlinear and total refractive index changes (RICs) and optical absorption coefficients (OACs) between the ground ($1s$) and the first excited state ($1p$) of CdSe/ZnTe core/shell quantum dot (CSQD) with Screened Modified Kratzer potential (SMKP): $V(r) = D_e \left(q - \frac{r_e e^{-\alpha r}}{r} \right)^2$ where r_e is the equilibrium bond length. To achieve this goal, the wave functions and the corresponding eigenvalues of the electron are investigated by resolving the time-independent Schrödinger equation using diagonalization technique in terms of the effective mass approximation. The dependency of energy difference between the $1s$ and $1p$ states and dipole transition matrix element on the SMKP parameters are examined. The numerical results exhibit that the characteristic parameters of SMKP (α , q and r_e) and incident optical intensity (I) have a strong impact on RICs and OACs. It was obtained that the resonance peak positions of the OACs and RICs are redshifted (blue shifted) with increasing the r_e (α and q parameters). Furthermore, to get a great variation of the RICs and OACs, a relatively feeble I should be adopted. The model potential used in the computation is important, and study of it will be practical in the development and research of nanostructures systems.

1 Introduction

The process for manufacturing nanoscale semiconductor has developed over the past years such as molecular beam epitaxy (MBE), Metalorganic vapor-phase epitaxy (MOVPE), etc. Then create various type of nanostructures from quantum well to QD with different shapes spherical, cylindrical, ring, ellipsoidal, cubic, etc. [1–6]. The QD materials with a controlled size and shape as well as the charge carriers are restricted in space, then causes major change in the physicochemical properties [3, 7–10], these properties aren't found in conventional materials. Many of the benefits come from the properties of the QD materials, which, as a result are taken attention by physicists, chemists, materials scientists, and recently, engineers and biologists. Consequently, it have been adopted to build and design the newest generation of semiconductor structures for manufacturing of a wide range of novel devices such as solar cell [11–13], light emitting diodes [14–16], biomedical applications [17–19], etc., with the best performances. The experimentally viable core/shell nanostructures system consists of a spherical QD made of one type of semiconductor material (which in this case represents the core) that is encased in another type of semiconductor material, also known as a shell. It should be noted that the efficiency of these materials is also affected by the elemental composition from which it is formed. The ZnTe and CdSe are promising II–VI direct-bandgap semiconductors with band gaps of 2.394 eV and 1.716 eV, respectively [20, 21]. The photoluminescence spectra result show that the intensity of CdSe QDs increases several times when the CdSe cores are sandwiched inside a large band gap shell material [22]. Moreover, the optical properties and luminescence of the as-synthesized nanocrystals can alter as a result of changes in the size and size distribution of the QDs [23], this behavior is a result of quantum confinement effects that is due to the spatial restrictions. Recently, the optical properties, especially the nonlinear ones, have been extensively investigated by experimental and theoretical scholars [24–30]. The optical properties of the nanostructure theoretically are based on the Schrödinger equation solution, in order to solve it, a lot of scientists have conducted many research work in order to solve it exactly or approximately with various potential interactions [31–34]. In this concern, the optical properties of this nanostructure are taken attention by several scholars,

^a e-mail: mohammed.jaouane@usmba.ac.ma

^b e-mail: elbakkari.kamal@gmail.com

^c e-mail: emrebahadiral@hotmail.com

^d e-mail: sali_ahm@yahoo.fr

^e e-mail: ungan@cumhuriyet.edu.tr (corresponding author)

in this regard, A. Cherni et al. have analyzed theoretically the optoelectronic properties of CdS quantum dot (QD) encapsulated in ZnSe matrix [35, 36]. A. Ed-Dahmouny et al. investigated the effect of electric field on the photoionization cross section of a donor impurity in GaAs/AlGaAs core/shell ellipsoidal quantum dots [37]. K.A. Rodríguez-Magdaleno et al. have studied effect of strain on the optical absorption coefficient of 1 s-1p transition for a spherical core shell [38], E. B. Al explored the effect of magnetic field on the absorption coefficient of a single dopant within the core/shell/shell QD for two intersubband $1s \rightarrow 1p$ and $1p \rightarrow 1d$ optical transitions by using the diagonalization method [39], M.R.K. Vahdani et al. [40] have computed the effect of dielectric constant on the CdSe/ZnS QD matrix. The aim of this work was to study the linear and nonlinear optical properties of CdSe/ZnTe CSQD where the potential confinement is modeling by the novelty potential titled the screened modified Kratzer potential. The organization of the work is the following, the Part 2 describes the studied system and the theoretical model used to achieve the optical properties: absorption coefficients and refractive indexes. In the Part 3, we discuss the obtained results of the CdSe/ZnTe CSQD. The conclusions are finally presented in Part 4.

2 Theory and calculation

Our model consists of an electron located in an isolated CdSe/ZnTe CSQD. This electron is evaluated under the Screened Modified Kratzer potential (SMKP). The electronic states and their corresponding energies are obtained by solving the time-independent Schrödinger equation, which can be written in a single band effective mass approximation as

$$\left[-\frac{\hbar^2}{2m^*} \nabla^2 + V(r) \right] \psi(r, \theta, \phi) = E \psi(r, \theta, \phi), \quad (1)$$

where the first term in parentheses is the contribution from the kinetic energy, \hbar is the reduced Planck constant, m^* represents the effective mass of the electron in the conduction band, and it is taken as m_c^* in the CdSe core and m_s^* in the ZnTe shell. The second term in parentheses represents SMKP [39] written as

$$V(r) = D_e \left(q - \frac{r_e e^{-\alpha r}}{r} \right)^2, \quad (2)$$

where D_e is the dissociation energy, r_e is the equilibrium bond length, α is the screening parameter, q is a control parameter whose selection is nonrandom, and r is the position of the electron relative to the dot center. The SMKP model is a general case of the modified Kratzer potential obtained for $q = 1$ and $\alpha = 0$, the inverse quadratic Yukawa potential is obtained by setting $q = 0$, and other potential models can be derived from the SMKP by varying the potential parameters. This type of potential is very important because it contains an attractive Coulomb term and a repulsive inverse-square barrier term. Because the overlap of these different types of potentials produces a pocket-like potential, and the shape of this potential is of great importance for studying the properties of quantum heterostructures.

In spherical coordinate, the Schrödinger Equation can be easily solved by separating the variables. Therefore, the wave function can be written as

$$\psi(r, \theta, \phi) = \varphi_{n,l}(r) Y_{l,m}(\theta, \phi), \quad (3)$$

where $\varphi_{n,l}(r)$ is the radial part of the envelope function and $Y_{l,m}(\theta, \phi)$ is the spherical harmonic function, n is the radial, l is angular momentum, and m ($-l \leq m \leq l$) is azimuth quantum numbers. The wave functions and the corresponding eigenenergies of the electron can be obtained using the diagonalization method applied in Ref [41]. Since spherical harmonics are the same for all spherically symmetric potentials, the shape of the potential only affects the radial wavefunction.

After the energies and the corresponding envelope wave functions are determined, the OACs and RICs can be calculated in the density matrix approach with [42, 43],

$$\alpha(\omega) = \omega \sqrt{\frac{\mu}{\varepsilon_r}} \text{Im}[\varepsilon_0 \chi(\omega)] \quad (4)$$

and

$$\frac{\Delta n(\omega)}{n_r} = \text{Re} \left[\frac{\chi(\omega)}{2n_r^2} \right], \quad (5)$$

respectively, where, μ is the magnetic permeability of the studied system, n_r is the refractive index of the semiconductor, ε_0 is the electric permittivity of free space, $\varepsilon_r = n_r^2 \varepsilon_0$ is the real part of the dielectric permittivity. The expression of first-order linear and third-order nonlinear optical sensitivity for transitions between two energy levels is given by

$$\chi_{\omega}^{(1)}(\omega) = \frac{\sigma_s |M_{ij}|^2}{\varepsilon_0 (E_{ij} - \hbar\omega - i\hbar\Gamma_{ij})} \quad (6)$$

and

$$\chi_{\omega}^{(3)}(\omega) = \frac{\sigma_s \hbar \omega |M_{ij}|^2 E^2}{\epsilon_0 (E_{ij} - \hbar \omega - i \hbar \Gamma_{ij})} \left[\frac{4 |M_{ij}|^2}{(E_{ij} - \hbar \omega)^2 + (\hbar \Gamma_{ij})^2} - \frac{|M_{jj} - M_{ii}|^2}{(E_{ij} - i \hbar \Gamma_{ij})(E_{ij} - \hbar \omega - i \hbar \Gamma_{ij})} \right], \tag{7}$$

where, σ_s represents the charge carrier density, $E_{ij} = \Delta E = E_i - E_j$ is the energy difference between the two states, $\Gamma_{ij} = 1/T_{ij}$ is the relaxation ratio, T_{ij} is the relaxation time, E is polarized monochromatic electromagnetic field interacts with the QD, M_{ij} is the electric dipole moment matrix element of the transition between the i and j states in QD. In the electric dipole approximation, if the polarization of electromagnetic radiation is chosen in the z -direction, the M_{ij} is given in the form,

$$M_{ij} = \langle \psi_i | e z | \psi_j \rangle, \tag{8}$$

where ψ_i and ψ_j are the eigenstates of the system, $z = r \cos \theta$ and e is the charge of the electron. In a dipole allowed optical transition, the angular momentum quantum numbers (l) of the respective states must have a difference of ± 1 . Therefore, we limit our study to the transition from the ground state ($l = 0, 1s$) to the first excited state ($l = 1, 1p$).

In a two-level system approach, the total OAC is theoretically formulated as

$$\alpha(\omega, I) = \alpha^{(1)}(\omega) + \alpha^{(3)}(\omega, I), \tag{9}$$

where

$$\alpha^{(1)}(\omega) = \sqrt{\frac{\mu}{\epsilon_r}} \frac{\sigma_s |M_{ij}|^2 \hbar \omega \Gamma_{ij}}{(E_{ij} - \hbar \omega)^2 + (\hbar \Gamma_{ij})^2} \tag{10}$$

and

$$\alpha^{(3)}(\omega, I) = -\sqrt{\frac{\mu}{\epsilon_r}} \frac{2I}{n_r \epsilon_0 c} \frac{\sigma_s |M_{ij}|^4 \hbar \omega \Gamma_{ij}}{[(E_{ij} - \hbar \omega)^2 + (\hbar \Gamma_{ij})^2]^2} \left[1 - \frac{|M_{jj} - M_{ii}|^2}{4 |M_{ij}|^2} \frac{3E_{ij}^2 - 4E_{ij} \hbar \omega + \hbar^2 (\omega^2 - \Gamma_{ij}^2)}{E_{ij}^2 + (\hbar \Gamma_{ij})^2} \right] \tag{11}$$

are linear and third-order nonlinear OACs, respectively, and I indicates the intensity of the incident electromagnetic field. In Eq. (11), near the resonant frequency, $M_{jj} - M_{ii}$ is zero for the electron in the QD. And furthermore, the resonance conditions for linear and third order nonlinear OACs are $\hbar \omega_1 = \sqrt{E_{ij}^2 + (\hbar \Gamma_{ij})^2}$ and $\hbar \omega_3 = \frac{1}{3} \left(E_{ij} + \sqrt{4E_{ij}^2 + 3(\hbar \Gamma_{ij})^2} \right)$, respectively. We define the following two functions associated with the resonance conditions:

$$\Omega_1 = e^{-2} \sqrt{E_{ij}^2 + (\hbar \Gamma_{ij})^2} |M_{ij}|^2 \tag{12}$$

and

$$\Omega_2 = \frac{e^{-4}}{3} \left(E_{ij} + \sqrt{4E_{ij}^2 + 3(\hbar \Gamma_{ij})^2} \right) |M_{ij}|^4. \tag{13}$$

Following these definitions, linear and nonlinear OACs at resonant frequency can be written as

$$\alpha^{(1)}(\omega) = \sqrt{\frac{\mu}{\epsilon_r}} \frac{\sigma_s \Gamma_{ij} e^2}{(E_{ij} - \hbar \omega)^2 + (\hbar \Gamma_{ij})^2} \Omega_1, \tag{14}$$

and

$$\alpha^{(3)}(\omega, I) = -\sqrt{\frac{\mu}{\epsilon_r}} \frac{2I}{n_r \epsilon_0 c} \frac{\sigma_s \Gamma_{ij} e^4}{[(E_{ij} - \hbar \omega)^2 + (\hbar \Gamma_{ij})^2]^2} \Omega_2 \tag{15}$$

Similarly, linear and nonlinear RICs are expressed analytically as

$$\frac{\Delta n^{(1)}(\omega)}{n_r} = \frac{\sigma_s |M_{ij}|^2}{2n_r^2 \epsilon_0} \frac{E_{ij} - \hbar \omega}{(E_{ij} - \hbar \omega)^2 + (\hbar \Gamma_{ij})^2} \tag{16}$$

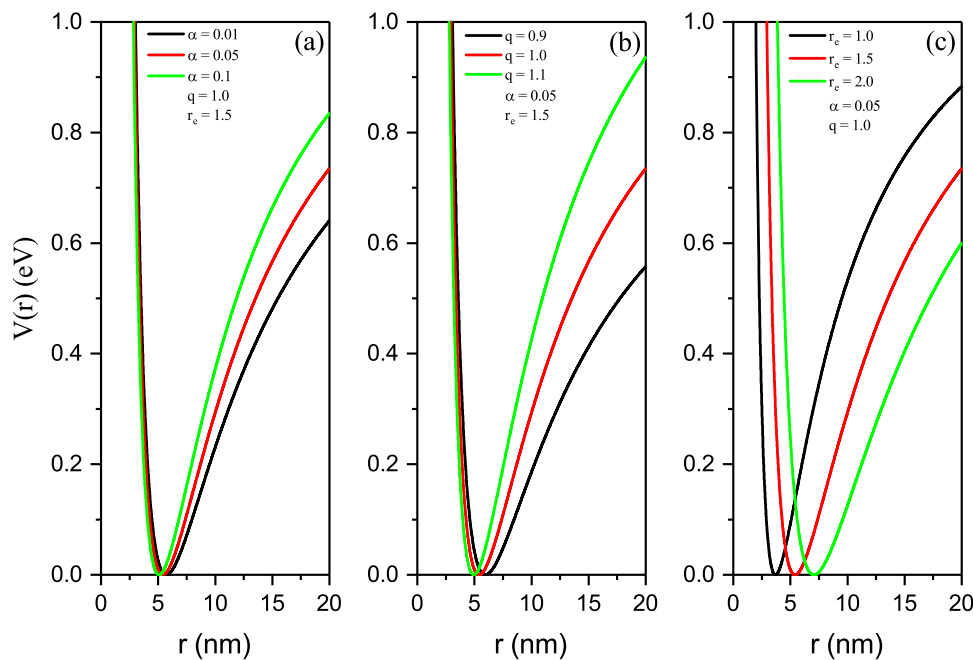
and

$$\frac{\Delta n^{(3)}(\omega, I)}{n_r} = \frac{-\mu c I \sigma_s |M_{ij}|^4}{n_r^3 \epsilon_0} \frac{E_{ij} - \hbar \omega}{[(E_{ij} - \hbar \omega)^2 + (\hbar \Gamma_{ij})^2]^2} \left[1 - \frac{|M_{jj} - M_{ii}|^2 \left[E_{ij}^2 - E_{ij} \left(\hbar \omega + \frac{(\hbar \Gamma_{ij})^2}{E_{ij} - \hbar \omega} \right) - 2(\hbar \Gamma_{ij})^2 \right]}{4 |M_{ij}|^2 [E_{ij}^2 + (\hbar \Gamma_{ij})^2]} \right], \tag{17}$$

Table 1 Some of the material parameters used in the calculations [38, 46]

	CdSe	ZnTe	The used values
Electron effective mass (m_0)	$m_c^* = 0.13$	$m_s^* = 0.15$	$m^* = \sqrt{m_c^* m_s^*} = 0.139$
Refractive index	$n_r^c = 2.5$	$n_r^s = 2.68$	$n_r = \sqrt{n_r^c n_r^s} = 2.59$

Fig. 1 SMKP as a function of r for various values of **a** α , **b** q and **c** r_e



where, c represents the speed of light in vacuum. In this context, the total RIC is given as

$$\frac{\Delta n(\omega, I)}{n_r} = \frac{\Delta n^{(1)}(\omega)}{n_r} + \frac{\Delta n^{(3)}(\omega, I)}{n_r} \tag{18}$$

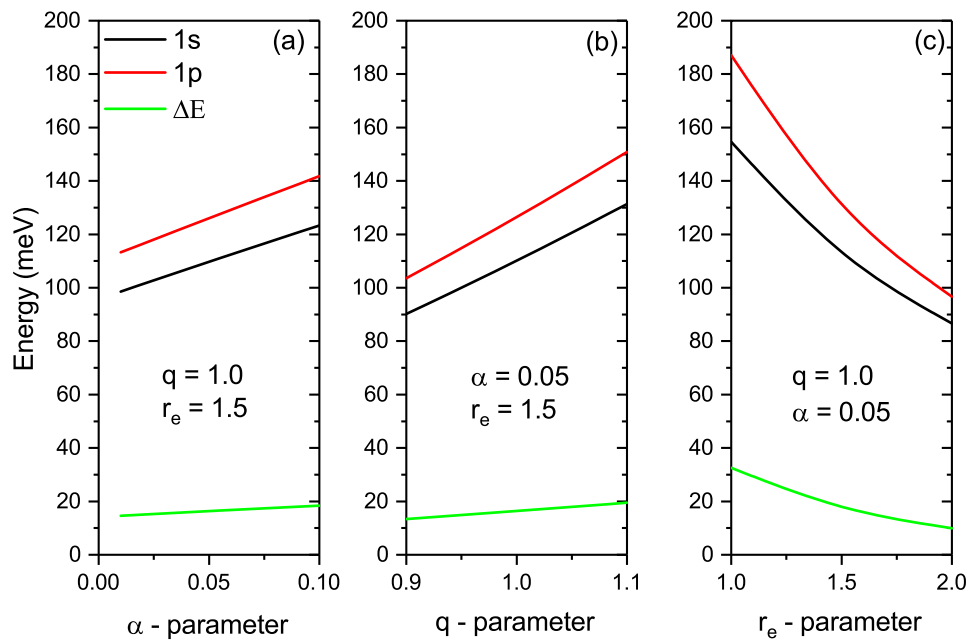
3 Results and discussion

In this section, we compute and plot the OACs and RICs of a spherical CdSe/ZnTe CSQD with SMKP. Some of the material parameters used in our calculations are listed in Table 1. We take the dissociation energy as $D_e = 1220\text{meV}$ [38, 44, 45]. Other parameters are as follows: $\sigma_s = 3 \times 10^{22}m^{-3}$, $\tau_{ij} = 0.25ps$.

In order to display the effect of the potential parameters (α, q and r_e) on the SMKP, we plot in Fig. 1 the variation of the shape of SMKP versus the distance r for various values of screening parameter α (a), control parameter q (b) and equilibrium bond length r_e (c). It can be verified that for smaller values of the distance r , the $V(r)$ becomes independent of variation of the parameters α and q , and which is only affected by the variation of r_e parameter in these regions. Also, we can see from the figure that the SMKP has a local minimum. Furthermore, the minimum point of the potential shifts to higher values of r with r_e , whereas it shifts slightly to the lower values of r with the increase of α or q , which indicates that the parameter r_e controls the minimum position of the SKMP more than the parameters α and q . On the other hand, we remark that an increase in the parameters α and q or a decrease in the r_e parameter and for higher values of r (edge right side of $V(r)$), the potential well moves to higher energies. It caused by the fact that the area of localization of the electron in the QD is increases (decreases) by the r_e (both parameters α and q). This figure indicate clearly that the effect of variation of these parameters could be significant in describing optical transition in the CdSe/ZnTe CSQD.

Before studying the linear and nonlinear optical properties in the CdSe/ZnTe CSQD, we shall examine the effect of the potential parameters (α, q and r_e) on the quantities controlling this optical response. Such quantities are the ground ($1s$), first excited state ($1p$), difference energy (ΔE), electric dipole moment matrix element (M_{ij}) and the two functions Ω_1 and Ω_2 (see Eqs. 12–13). Then, Fig. 2a–c displays the variations in ground, first excited state and difference energy ΔE as a functions of the potential parameters (α, q and r_e). The results are given in every figure by changing one parameter and keeping the others fixed. In all cases, it can be seen that the values of the ground state level are lower than those the first excited one, owing to the strong confinement of the wavefunction of the latter. Moreover, we can notice that the increment in the parameters α and q introduces an increases of the energy levels and the ΔE . This is due to the fact that the increment of α and q parameters offers a more confinement effect. On the other hand, the energy between the $1s$ and $1p$ states diminished as r_e increases, as it is shown in panel (c) of Fig. 2, which gives a weakening in

Fig. 2 The ground-1s, first excited state-1p and difference energy- ΔE as a function of **a** α , **b** q and **c** r_e



confinement of the electron in the core/shell and this is in agreement with the behavior of the SMKP in Fig. 1c. These results can be explained by the fact that the two lowest subband energy levels get closer (farther) to each other, consequently the ΔE decreases with r_e (increases with α and q). Note that the energy levels and ΔE are more sensitive to the variation of the r_e parameter and consequently will be reflected in the OAC peak location, as will be discussed below.

In Fig. 3a–c, the electric dipole moment matrix element M_{ij} and the two functions (Ω_1, Ω_2) are presented for the similar configuration as Fig. 2. According to Eqs. (14–15), it is evident that the change of the factor $\Omega_1(\Omega_2)$ affects the peak amplitude of the linear (nonlinear) OACs. The observation shows that there is no important change in the Ω_1 with the parameters α and q , whereas there is a slight diminution of this function with r_e . Additionally, the increase of α and q parameters (r_e parameter) reduces (enhances) the function Ω_2 . In addition, the augmentation in confinement of the electron by the increases in the parameters α and q brings about a reduction in the dipole matrix element M_{ij} as observed in panels (a) and (b) of Fig. 3. On the other hand, the r_e parameter has an opposite effect. Indeed, the matrix element M_{ij} increase with r_e which gives an augmentation of the spatial overlap of the corresponding envelope wavefunction. Also we can see that for the fixed parameters at $q = 1.0$ and $\alpha = 0.05$, the value of dipole matrix element is greater for higher r_e values (Fig. 3c). These found numerical results (Figs. 2 and 3) are the basis for the physical description for the maxima and minima and energy position of resonant peaks of linear, nonlinear and total OACs and RICs.

The variation of the linear (dashed), nonlinear (dotted), and total (solid) OACs for the $1s \rightarrow 1p$ transition versus incident photon energy $\hbar\omega$ are drawn in Fig. 4a–c for various values of α, q and r_e respectively with optical intensity $I = 400 MW/m^2$. When the incident photon energy $\hbar\omega$ equals the difference energy ΔE , the third-order nonlinear OAC has a minimum, while the total and the linear OACs present a maximum. Also, the total OAC is very dependent on the decreasing and increasing of the nonlinear and linear OACs and it is always lesser than the linear OAC. In Fig. 4a, while the parameters q and r_e are keeping constant ($q = 1.0$ and $r_e = 1.5$), the value of the parameter α is changed as 0.01, 0.05 and 0.1. It can be observed that the amplitude of linear OAC is almost constant with the variation of the parameter α . Whereas, when we look at the peak amplitude of the nonlinear optical absorption, as the parameter α increase, the amplitude of the peak decreases slightly. With the effect of this decrease, the peak amplitude of the total OAC increases with the increasing of the parameter α . These results are related to the functions Ω_1 and Ω_2 given in Fig. 3a. Furthermore, the peaks of nonlinear, linear as well as total OACs shift slightly to the higher energies (blue shift) with the increasing of parameter α . This fact can be explained by the increasing energy difference between $1s$ and $1p$ states caused by the increasing of the α as seen from Fig. 2a. In addition, we observe in Fig. 4b the same behavior of variation peaks of OACs under the variation of parameter q . In Fig. 4c, while the parameters α and q are keeping constant ($q = 1.0$ and $\alpha = 0.05$), the value of the parameter r_e is changed as 1.0, 1.5 and 2.0. It can be found that the peak magnitude of the total OAC decreases as the parameter r_e increases. This result is related to the variation of the functions Ω_1 and Ω_2 as before mentioned. Additionally, the position of the resonant peak shows a redshift as the parameter r_e increases, which is completely agree with the dependence of parameter r_e on the transition energy reported in Fig. 2c. The physical reason for this feature is that as parameter r_e increases, the energy difference between the first two lower-lying energy levels decreases.

We have plotted in Fig. 5 the variation of linear (dashed), nonlinear (dotted) and total (solid) RICs for the $1s \rightarrow 1p$ transition as a function of photon energy $\hbar\omega$ for various values of α (a), q (b) and r_e (c). The conditions used for Fig. 4 are the same as in this

Fig. 3 Values of M_{ij} , Ω_1 and Ω_2 as a function of **a** α , **b** q and **c** r_e

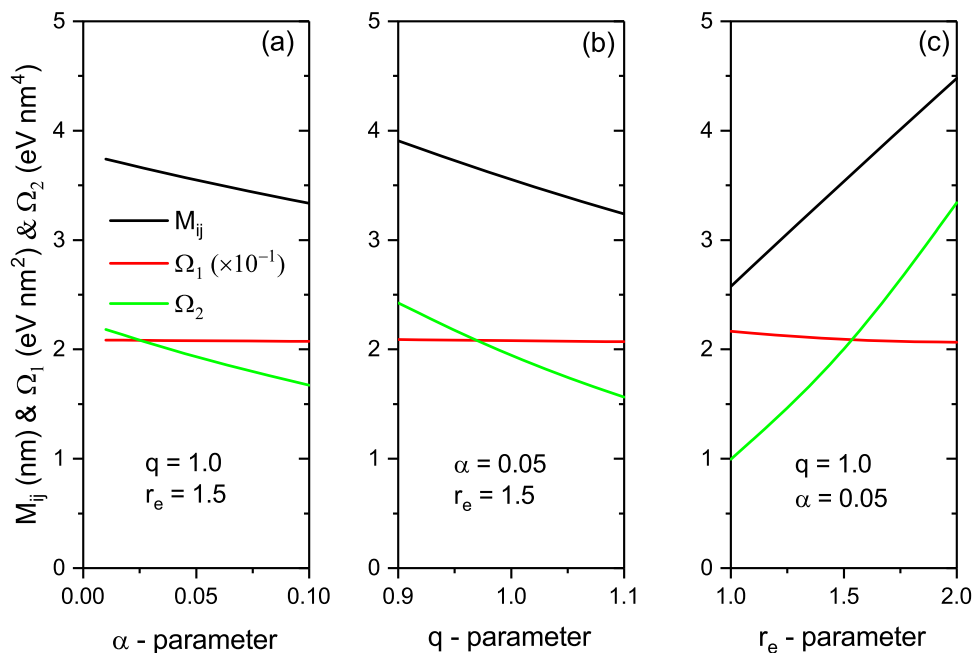


Fig. 4 Linear (dashed), nonlinear (dotted), and total (solid) OACs for the $1s \rightarrow 1p$ transition as a function of photon energy at different values of **a** α , **b** q and **c** r_e . $I = 400 MW/m^2$

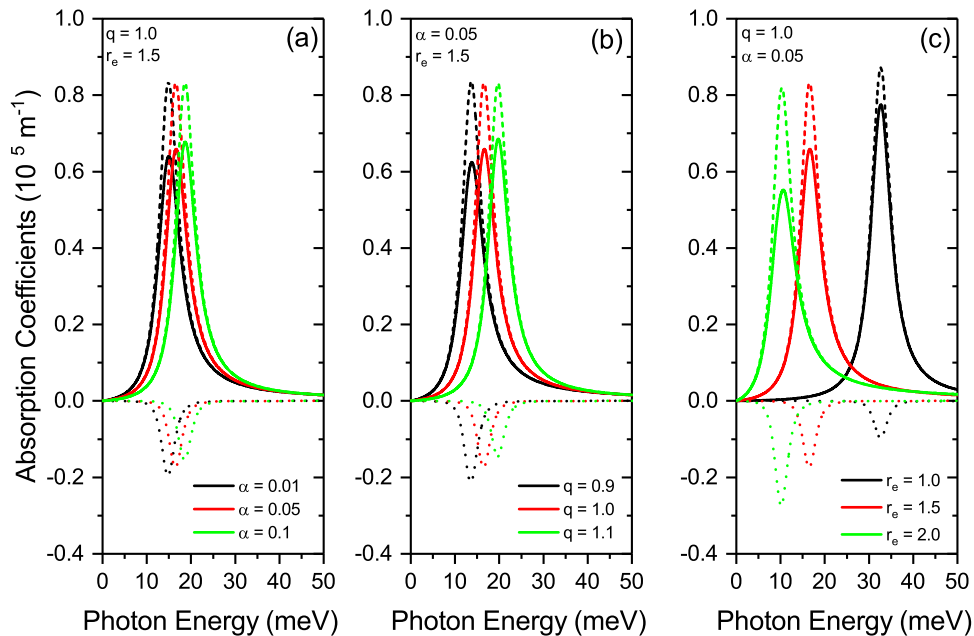


figure. One may clearly notice that the growing of α and q (r_e) leads to a variation of the minima and maxima of peaks position of the RICs shifting to the higher (lower) energies with reduction (augmentation) of the magnitude of the resonant peaks. In addition, the parameter r_e has a significant effect on the position of the resonant peak compared to the influence of the parameters q and α . This behavior can be explicated by the energy difference ΔE , as can be seen in Fig. 2. Looking at Eqs. 16 and 17, it can be seen that the peak amplitude of linear (nonlinear) RICs is directly proportional to the square (fourth order) of M_{ij} , and thus the amplitude changes with the changing parameters are consistent with the change of M_{ij} given in Fig. 3. The results of the analysis found in this figure are well-matched with Fig. 4.

Finally, in Fig. 6a–b we have depicted the total OAC and RIC as a function of photon energy for seven different values of incident optical intensities I , respectively, with the following fixed parameters $a = 0.05$, $q = 1.0$ and $r_e = 1.5$. From Eqs. (9)–(18), we note that the linear OAC and RIC do not depend on the I , while the nonlinear OAC and RIC depend linearly on the incident optical intensities. Because of this, we have observed clearly that the amplitude of the total OAC and RIC decrease with an increase in the incident optical intensity, due to the negative contribution of the nonlinear term. Thus, to get a great variation of the refractive index and optical absorption, a relatively feeblor I should be adopted. Furthermore, when I reaches a critical value, two peaks are observed

Fig. 5 Linear (dashed), nonlinear (dotted), and total (solid) RICs for the $1s \rightarrow 1p$ transition as a function of photon energy at different values of **a** α , **b** q and **c** r_e . $I = 400 \text{ MW/m}^2$

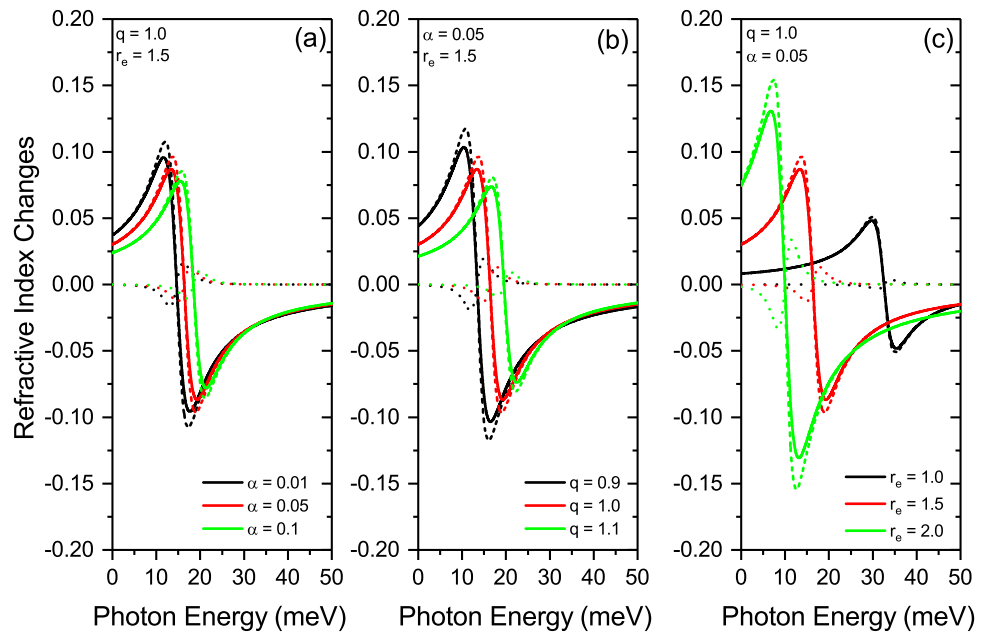
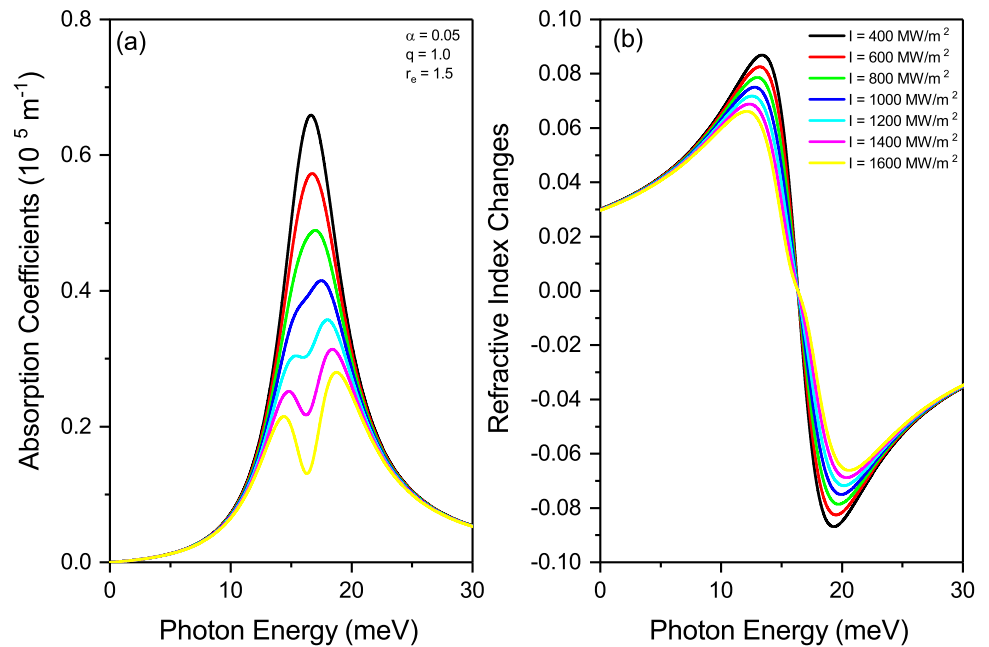


Fig. 6 a Total OAC and **b** Total RIC at different I values as a function of photon energy



in the total OAC (bleaching). These outcomes are in agreement with investigation in Ref [47], related to an electron in a spherical QD. Note that the position of the resonance peak of total OAC is not affected by the variation of I . This finding is in agreement with the works in Refs. [48–50]. In addition, by varying the I , the peak position of the total RIC changes slightly. Therefore, our numerical investigations would help readers understand the effects of varying the incident optical intensity and modified Kratzer potential on the linear and nonlinear optical properties of CdSe/ZnTe CSQDs.

4 Conclusion

Summarizing, we have calculated the difference energy (ΔE) between the ground ($1s$) and the first excited state ($1p$), dipole transition matrix element, linear, nonlinear and total optical absorption coefficients and refractive index changes for CdSe/ZnTe core/shell quantum dots with Screened Modified Kratzer potential. From our numerical results it is found that the examined quantities are modified by the parameters of Screened Modified Kratzer potential (α , q and r_e) as well as the incident optical intensity (I). The results found display the following: increasing the parameters α and q in the Screened Modified Kratzer potential or decreasing

the parameter r_e , the total optical absorption coefficient and refractive index change shift to higher photon energies (blue shift). The parameter r_e has a remarkable effect on the position of the resonant peak compared to the influence of the parameters q and α . The amplitude of total optical absorption coefficient and refractive index change decrease with an increase in I and the position of the resonance peak of optical absorption coefficient is not affected by the variation of the incident optical intensity. Lastly, we hope that the present investigation will give to a better understanding linear and nonlinear optical properties of core/shell and other nanostructures.

Data availability statement This manuscript has associated data in a data repository. [Authors' comment: Data will be made available on request.]

References

1. K. El-Bakkari, A. Sali, E. Iqraoun, A. Ezzarfi, Polaron and conduction band non-parabolicity effects on the binding energy, diamagnetic susceptibility and polarizability of an impurity in quantum rings. *Superlattices Microstruct.* **148**, 106729 (2020). <https://doi.org/10.1016/j.spmi.2020.106729>
2. K. El-Bakkari, A. Sali, E. Iqraoun, A. Rezzouk, N. Es-Sbai, M. Ouazzani Jamil, Effects of the temperature and pressure on the electronic and optical properties of an exciton in GaAs/Ga $_{1-x}$ Al $_x$ As quantum ring. *Phys. B Condens. Matter.* **538**, 85–94 (2018). <https://doi.org/10.1016/j.physb.2018.03.010>
3. E. Kasapoglu, F. Ungan, H. Sari, I. Sökmen, M.E. Mora-Ramos, C.A. Duque, Donor impurity states and related optical responses in triangular quantum dots under applied electric field. *Superlattices Microstruct.* **73**, 171–184 (2014). <https://doi.org/10.1016/j.spmi.2014.05.023>
4. M. Sayrac, E. Kaynar, F. Ungan, The effect of structure parameters and static electric field on the nonlinear optical properties of triple InGaAs / GaAs quantum well. *J. Mol. Struct.* **1273**, 134252 (2023). <https://doi.org/10.1016/j.molstruc.2022.134252>
5. A. Sali, M. Fliyou, H. Satori, H. Loumrhari, Photoionization of impurities in quantum well wire. *Phys. Status Solidi.* **1**, 661–670 (1999)
6. R. Arraoui, A. Sali, A. Ed-Dahmouny, M. Jaouane, A. Fakkahi (2021) Polaronic mass and non-parabolicity effects on the photoionization cross section of an impurity in a double quantum dot. *Superlattices Microstruct.* 159: 107049. DOI: <https://doi.org/10.1016/j.spmi.2021.107049>.
7. M. Jaouane, A. Sali, A. Fakkahi, R. Arraoui, A. Ed-Dahmouny, F. Ungan (2022) Photoionization cross section of donor single dopant in multilayer quantum dots under pressure and temperature effects. *Phys E Low-Dimensional Syst Nanostructures.* 144: 115450. DOI: <https://doi.org/10.1016/j.physe.2022.115450>.
8. M. Jaouane, A. Sali, A. Ezzarfi, A. Fakkahi, R. Arraoui, Study of hydrostatic pressure, electric and magnetic fields effects on the donor binding energy in multilayer cylindrical quantum dots. *Phys. E Low-Dimensional Syst. Nanostructures.* (2021). <https://doi.org/10.1016/j.physe.2020.114543>
9. A. Ed-Dahmouny, A. Sali, N. Es-Sbai, R. Arraoui, M. Jaouane, A. Fakkahi, K. El-Bakkari, C.A. Duque (2022) Combined effects of hydrostatic pressure and electric field on the donor binding energy, polarizability, and photoionization cross-section in double GaAs/Ga $_{1-x}$ Al $_x$ As quantum dots, *Eur. Phys. J. B.* 95:8. DOI: <https://doi.org/10.1140/epjb/s10051-022-00400-2>.
10. A. Fakkahi, A. Sali, M. Jaouane, R. Arraoui, A. Ed-Dahmouny (2022) Study of photoionization cross section and binding energy of shallow donor impurity in multilayered spherical quantum dot. *Phys. E Low-Dimensional Syst. Nanostructures.* 143: 115351. DOI: <https://doi.org/10.1016/j.physe.2022.115351>.
11. J. Jasieniak, B.I. MacDonald, S.E. Watkins, P. Mulvaney, Solution-processed sintered nanocrystal solar cells via layer-by-layer assembly. *Nano Lett.* **11**, 2856–2864 (2011). <https://doi.org/10.1021/nl201282v>
12. C. Yuan, L. Li, J. Huang, Z. Ning, L. Sun, H. Ågren, Improving the photocurrent in quantum-dot-sensitized solar cells by employing alloy PbxCd $_{1-x}$ S quantum dots as photosensitizers. *Nanomaterials.* **6**, 87 (2016). <https://doi.org/10.3390/nano6060097>
13. M. Jaouane, A. Fakkahi, A. Ed-Dahmouny, K. El-Bakkari, A.T. Tuzemen, R. Arraoui, A. Sali, F. Ungan, Modeling and simulation of the influence of quantum dots density on solar cell properties, *Eur. Phys. J. Plus.* 138 (2023) 148. DOI: <https://doi.org/10.1140/epjp/s13360-023-03736-5>.
14. Q. Sun, Y.A. Wang, L.S. Li, D. Wang, T. Zhu, J. Xu, C. Yang, Y. Li, Bright, multicoloured light-emitting diodes based on quantum dots. *Nat. Photonics.* **1**, 717–722 (2007). <https://doi.org/10.1038/nphoton.2007.226>
15. X. Dai, Z. Zhang, Y. Jin, Y. Niu, H. Cao, X. Liang, L. Chen, J. Wang, X. Peng, Solution-processed, high-performance light-emitting diodes based on quantum dots. *Nature* **515**, 96–99 (2014). <https://doi.org/10.1038/nature13829>
16. W. Chen, K. Wang, J. Hao, D. Wu, S. Wang, J. Qin, C. Li, W. Cao, Highly efficient and stable luminescence from microbeams integrated with Cd-Free quantum dots for white-light-emitting diodes. *Part. Part. Syst. Charact.* **32**, 922–927 (2015). <https://doi.org/10.1002/ppsc.201500074>
17. K. Susumu, B.C. Mei, H. Mattoussi, Multifunctional ligands based on dihydrolipoic acid and polyethylene glycol to promote biocompatibility of quantum dots. *Nat. Protoc.* **4**, 424–436 (2009). <https://doi.org/10.1038/nprot.2008.247>
18. L. Ye, K.T. Yong, L. Liu, I. Roy, R. Hu, J. Zhu, H. Cai, W.C. Law, J. Liu, K. Wang, J. Liu, Y. Liu, Y. Hu, X. Zhang, M.T. Swihart, P.N. Prasad, A pilot study in non-human primates shows no adverse response to intravenous injection of quantum dots. *Nat. Nanotechnol.* **7**, 453–458 (2012). <https://doi.org/10.1038/nnano.2012.74>
19. D. Gao, P. Zhang, Z. Sheng, D. Hu, P. Gong, C. Chen, Q. Wan, G. Gao, L. Cai, Highly bright and compact alloyed quantum rods with near infrared emitting: a potential multifunctional nanoplatfor for multimodal imaging in vivo. *Adv. Funct. Mater.* **24**, 3897–3905 (2014). <https://doi.org/10.1002/adfm.201304225>
20. W. Shan, W. Walukiewicz, J.W. Ager, K.M. Yu, J. Wu, E.E. Haller, Pressure dependence of the fundamental band-gap energy of CdSe. *Appl. Phys. Lett.* **84**, 67–69 (2004). <https://doi.org/10.1063/1.1638879>
21. J. Singh, *Semiconductor optoelectronics: physics and technology* (McGraw-Hill, 1995)
22. A.P.P.R. Joël Bleuse, Highly luminescent CdSe/ZnSe Core/shell nanocrystals of low size dispersion. *Nano Lett.* **2**, 781–784 (2002). <https://doi.org/10.1021/nl025596y>
23. Z. Lin, A. Franceschetti, M.T. Lusk, Size dependence of the multiple exciton generation rate in CdSe quantum dots. *ACS Nano* **5**, 2503–2511 (2011). <https://doi.org/10.1021/nn200141f>
24. S. Sakiroglu, D.G. Kilic, U. Yesilgul, F. Ungan, E. Kasapoglu, H. Sari, I. Sokmen, Third-harmonic generation of a laser-driven quantum dot with impurity. *Phys. B Condens. Matter.* **539**, 101–105 (2018). <https://doi.org/10.1016/j.physb.2018.04.005>
25. A.T. Tuzemen, H. Dakhloui, M.E. Mora-Ramos, F. Ungan, The nonlinear optical properties of GaAs/GaAlAs triple quantum well: role of the electromagnetic fields and structural parameters. *Phys. B Condens. Matter.* **646**, 414286 (2022). <https://doi.org/10.1016/j.physb.2022.414286>
26. F. Ungan, M.K. Bahar, M.G. Barseghyan, L.M. Pérez, D. Laroze, Effect of intense laser and electric fields on nonlinear optical properties of cylindrical quantum dot with Morse potential. *Optik (Stuttg.)* **236**, 78 (2021). <https://doi.org/10.1016/j.ijleo.2021.166621>

27. A. Fakkahi, A. Sali, M. Jaouane, R. Arraoui, A. Ed-Dahmouny, Investigation of the nonlinear optical rectification coefficient in a multilayered spherical quantum dot, *Opt. Mater. (Amst)*. **132** (2022) 112752. DOI: <https://doi.org/10.1016/j.optmat.2022.112752>.
28. H. Kumar, R.R. Singh, Approach to advance optical properties in CdS/ZnS and ZnS/CdS core/shell nanostructures through shell alteration. *Phys. E Low-Dimensional Syst. Nanostruct.* **108**, 281–287 (2019). <https://doi.org/10.1016/j.physe.2018.12.023>
29. M. Jaouane, A. Sali, A. Fakkahi, R. Arraoui, F. Urgan, The effects of temperature and pressure on the optical properties of a donor impurity in (In, Ga)N/GaN multilayer cylindrical quantum dots, *Micro and Nanostructures. Micro and Nanostructures*. **163**, 107146 (2022). <https://doi.org/10.1016/j.spmi.2021.107146>
30. A. Ed-Dahmouny, A. Sali, N. Es-Sbai, R. Arraoui, C.A. Duque, The impact of hydrostatic pressure and temperature on the binding energy, linear, third-order nonlinear, and total optical absorption coefficients and refractive index changes of a hydrogenic donor impurity confined in GaAs/AlxGa1-xAs double quantum dots, *Eur. Phys. J. Plus*. **137**: (2022) 784. DOI: <https://doi.org/10.1140/epjp/s13360-022-03002-0>.
31. A. Fakkahi, A. Sali, M. Jaouane, R. Arraoui, Hydrostatic pressure, temperature, and electric field effects on the hydrogenic impurity binding energy in a multilayered spherical quantum dot. *Appl. Phys. A*. **127**, 908 (2021). <https://doi.org/10.1007/s00339-021-05055-x>
32. A. Tiutiunnyk, V. Akimov, V. Tulupenko, M.E. Mora-Ramos, E. Kasapoglu, F. Urgan, I. Sökmen, A.L. Morales, C.A. Duque, Electronic structure and optical properties of triangular GaAs/AlGaAs quantum dots: exciton and impurity states. *Phys. B Condens. Matter*. **484**, 95–108 (2016). <https://doi.org/10.1016/j.physb.2015.12.045>
33. A. Sali, H. Satori, The combined effect of pressure and temperature on the impurity binding energy in a cubic quantum dot using the FEM simulation. *Superlattices Microstruct.* **69**, 38–52 (2014). <https://doi.org/10.1016/j.spmi.2014.01.011>
34. M. Jaouane, A. Sali, E. Kasapoglu, F. Urgan, Tuning of nonlinear optical characteristics of a cylindrical quantum dot by external fields and structure parameters. *Philos. Mag.* **1**, 19 (2023). <https://doi.org/10.1080/14786435.2023.2171499>
35. A. Cherni, N. Yahyaoui, N. Zeiri, M. Said, S. Saadaoui, Simultaneous effect of the capped matrix and the geometric factors of CdS/ZnSe spheroidal quantum dots on the linear and nonlinear optical properties. *Opt. Quantum Electron.* **55**, 273 (2023). <https://doi.org/10.1007/s11082-023-04545-x>
36. A. Cherni, N. Zeiri, N. Yahyaoui, A. Jbeli, S.A.-B. Nasrallah, M. Said, Tuning of nonlinear optical properties by size and photonic intensity in CdS/ZnSe core/shell quantum dot-matrix pattern. *J. Nonlinear Opt. Phys. Mater.* **32**, 78 (2023). <https://doi.org/10.1142/S021886352350011X>
37. A. Ed-Dahmouny, N. Zeiri, A. Fakkahi, R. Arraoui, M. Jaouane, A. Sali, N. Es-Sbai, K. El-Bakkari, C.A. Duque, Impurity photo-ionization cross section and stark shift of ground and two low-lying excited electron-states in a core/shell ellipsoidal quantum dot, *Chem. Phys. Lett.* **812** (2023) 140251. DOI: <https://doi.org/10.1016/j.cplett.2022.140251>.
38. A. Naifar, N. Zeiri, S.A. Nasrallah, M. Said, Optik Optical properties of CdSe / ZnTe type II core shell nanostructures. *Opt. - Int J. Light Electron Opt.* **146**, 90–97 (2017). <https://doi.org/10.1016/j.ijleo.2017.08.079>
39. E.B. Al, L. Hitler, B.I. Ita, P.A. Isa, N.-I. Nelson, I. Joseph, O. Ivan, T.O. Magu, Wkb solutions for inversely quadratic Yukawa plus inversely quadratic Hellmann potential, *World. J. Appl. Phys.* **2**, 109–112 (2017). <https://doi.org/10.1007/s11082-021-03340-w>
40. M.R.K. Vahdani, N. Ehsanfard, Nonlinear optical properties of a slab of CdSe/ZnS quantum dot matrix. *Phys. B Condens. Matter*. **548**, 1–9 (2018). <https://doi.org/10.1016/j.physb.2018.08.006>
41. E.B. Al, H. Sari, Binding Energy And Absorption of Donor Impurity In Spherical GaAs / AlxGa1-x As Quantum Dots With Konwent Potential, (2021) 0–13.
42. E.B. Al, Effect of size modulation and donor position on intersubbands refractive index changes of a donor within a spherical core/shell/shell semiconductor quantum dot. *Cumhur. Sci. J.* **42**, 694–701 (2021). <https://doi.org/10.17776/cs.j.927289>
43. C.O. Edet, E.B. Al, F. Urgan, N. Ali, N. Rusli, S.A. Aljunid, R. Endut, M. Asjad, Effects of applied magnetic field on the optical properties and binding energies spherical gaas quantum dot with donor impurity. *Nanomaterials* **12**, 2741 (2022). <https://doi.org/10.3390/nano12162741>
44. A. Naifar, N. Zeiri, S.A. Nasrallah, M. Said, Photonics and nanostructures - fundamentals and applications linear and nonlinear optical properties of CdSe / ZnTe core / shell spherical quantum dots embedded in different dielectric matrices. *Photonics Nanostructures - Fundam. Appl.* **40**, 100789 (2020). <https://doi.org/10.1016/j.photonics.2020.100789>
45. E.T. Yu, M.C. Phillips, J.O. Mccaldin, T.C. McGill, Measurement of the CdSe / ZnTe valence band offset by xray photoelectron spectroscopy Measurement of the CdSe / ZnTe valence band offset by x-ray photoelectron spectroscopy, **2233** (2012). DOI: <https://doi.org/10.1116/1.585726>.
46. A. Chafai, I. Essaoudi, A. Ainane, R. Ahuja, Linear and nonlinear optical properties of donors inside a CdSe/ZnTe core/shell nanodot: Role of size modulation. *Results Phys.* (2019). <https://doi.org/10.1016/j.rinp.2019.102414>
47. C.P. Onyenegecha, Linear and nonlinear optical properties in spherical quantum dots: Modified Möbius squared potential. *Heliyon*. **8**, e10387 (2022). <https://doi.org/10.1016/j.heliyon.2022.e10387>
48. L. Máthé, C.P. Onyenegecha, A.A. Farcaş, L.M. Pioraş-Ţimbolmaş, M. Solaimani, H. Hassanabadi, Linear and nonlinear optical properties in spherical quantum dots: Inversely quadratic Hellmann potential, *Phys. Lett. Sect. A Gen. At. Solid State Phys.* **397** (2021). DOI: <https://doi.org/10.1016/j.physleta.2021.127262>.
49. G.A. Mantashian, N.A. Zaqaryan, P.A. Mantashyan, H.A. Sarkisyan, S. Baskoutas, D.B. Hayrapetyan, Linear and nonlinear optical absorption of cdse/cds core/shell quantum dots in the presence of donor impurity. *Atoms*. **9**, 1–10 (2021). <https://doi.org/10.3390/atoms9040075>
50. J. Huang, Effect of the charges of impurity on the refractive index changes in parabolic quantum dot. *Phys. B Condens. Matter*. **409**, 16–20 (2013). <https://doi.org/10.1016/j.physb.2012.10.007>

Springer Nature or its licensor (e.g. a society or other partner) holds exclusive rights to this article under a publishing agreement with the author(s) or other rightsholder(s); author self-archiving of the accepted manuscript version of this article is solely governed by the terms of such publishing agreement and applicable law.